Rapid communication

Ti–6Al–4V with micro- and macropores produced by powder sintering and electrochemical dissolution of steel wires

Daniel J. Jorgensen*, David C. Dunand

Department of Materials Science and Engineering, Northwestern University, Evanston, IL, 60208, USA

ABSTRACT

Ti–6Al–4V powder preforms containing parallel layers of steel wire meshes are sintered into composites. Elongated macropores are created by electrochemical dissolution of the steel wires, and equiaxed micropores by partial powder densification. The macropore diameter and fraction is tailored by the creation of a Fe-containing diffusion zone in the Ti–6Al–4V matrix, which is removed electrochemically together with the wires. Ti–6Al–4V with 21–41% porosity shows compressive stiffness and strength attractive for biomedical implants.

© 2009 Elsevier B.V. All rights reserved.

Commercial purity titanium (CP-Ti) and Ti–6Al–4V are widely used as medical implants because of their excellent surface oxide biocompatibility, corrosion resistance and strength [1]. The high stiffness of the implant can however cause stress shielding, leading to deterioration of the bone [2]. Reducing the implant stiffness to values closer to that of bone can be achieved by introduction of porosity; furthermore, if pores have sizes in the 200–500 μm range, they provide opportunities for bone ingrowth, improving implant anchorage [3]. Current powder-metallurgy methods for producing porous titanium, as reviewed in Ref. [4], include partial sintering of powders [5] or fibers [6], sintering of hollow powders [7], creep expansion of gas-filled pores [8–10], sintering of powders in the presence of fugitive space-holders [11], direct laser/electron beam fabrication [12,13], electro-discharge-sintering [14], gel-casting [15,16] and freeze casting of powder slurries [17]. Recently, Kwok et al. [18] described a new process where CP-Ti powders are sintered in the presence of steel spheres, wires, or meshes, which are subsequently removed electrochemically, while the CP-Ti matrix is cathodically protected. The goal of the present paper is to create, for the first time, samples with three-dimensional porosity by this method, allowing mechanical testing. Another goal is to demonstrate this new method for Ti–6Al–4V, which is the main biomedical titanium alloy [1].

The Ti–6Al–4V powders used here exhibited an oxygen content of 0.17 wt.%, a size of 44–53 μm and an angular shape, as

expected from the hydride–dehydride production method reported by the manufacturer (Phelly Materials, Bergenfield, NJ) (Fig. 1). The steel mesh (from McMaster-Carr, Elmhurst, IL) consisted of 356 μm diameter low-carbon steel wires woven in an orthogonal pattern, with wire center-to-center spacing of 1067 μm in each direction, and an open area of 44% (Fig. 2). Six layers of 0.45 g of Ti–6Al–4V powders were poured and hand-compacted, alternating with five layers of mesh, in a 12.7 mm inside diameter die. After cold-compaction at 350 MPa for 5 min, the green samples were loaded into a vacuum furnace with base pressure $<5 \times 10^{-6}$ torr, heated to 1050 °C at a rate of 10 °C/min and sintered for 24 h, as described in more detail below.

Previous work [19] showed that steel with >0.2 wt.% carbon, when in intimate contact with CP-Ti during heat-treatment or sintering, forms at its surface a thin, continuous TiC layer which inhibits Fe–Ti interdiffusion. Steel with lower carbon content allows iron to diffuse deeply into the titanium matrix at 800–1000 °C. As shown by Kwok et al. [18] in CP-Ti, the TiC layer prevents interdiffusion between steel and titanium during the densification operation, so that pores, after electrochemical steel removal, replicate exactly the shape and size of the original steel spheres or wires. For lower carbon steel with diffusion of iron into titanium, however, the steel wires and the surrounding Fe-containing titanium matrix are removed electrochemically, resulting in larger pore diameter and thus higher porosity.

Here, three sets of samples were sintered, referred to as high-interdiffusion (HI), intermediate-interdiffusion (II), and low-interdiffusion (LI). The HI samples contained the as-received steel meshes with 0.13 wt.% carbon and were sintered for 24 h at 1050 °C, allowing extensive diffusion of Fe into the Ti–6Al–4V matrix. The II samples were sintered for 6 h, to obtain about half the Fe dif-

* Corresponding author. Present address: 2238 University Dr., Naperville, IL 60565, USA. Tel.: +1 630 740 3446; fax: +1 847 491 7820.
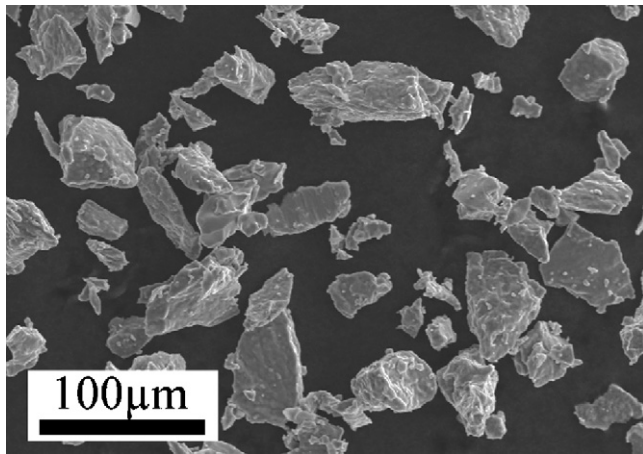*E-mail addresses:* DanielJorgensen2009@u.northwestern.edu (D.J. Jorgensen), dunand@northwestern.edu (D.C. Dunand).

Fig. 1. SEM image of Ti–6Al–4V powders with angular shape.

Fig. 3. EDX profiles of iron content along a radial direction from steel wire in sintered samples. The origin is at the wire/matrix interface and the Fe concentration is normalized to the maximum Fe concentration in the wire.

fusion distance of the previous HI samples. After the steel was electrochemically removed, these II samples were sintered for an additional 18 h to obtain the same total sintering time. Finally, the LI samples, which were also sintered for 24 h at 1050 °C, contained steel meshes which had been first carburized in a graphite pack in air at 960 °C for 1 h to achieve a carbon content of 0.67 wt.% C (as measured by Wah Chang Analytical Laboratory Services, Albany, OR).

Fig. 3 shows Fe diffusion profiles in the Ti–6Al–4V matrix measured by energy dispersive X-ray analysis carried out in a scanning electron microscope (SEM) at 25 kV. It is apparent that Fe diffusion in the matrix is almost completely inhibited for the LI sample, as previously observed during sintering of CP-Ti powders [18], and as expected from the continuous TiC layer at the steel–titanium interface (Fig. 4). In the II sample, no TiC is visible, as expected from the low-carbon content of the wires; the iron content drops at the wire/matrix interface to a concentration of 0.2 (value normalized with respect to the pure Fe wire), and decreases steadily to zero after an estimated length of ~290 μm (Fig. 3). In the HI sample, the iron content drops to the same 0.2 normalized concentration (probably corresponding to the maximum saturation of Ti with Fe) and decreases to zero over a longer diffusion length. Fig. 5(a) shows a LI sample with no interdiffusion zone visible in the etched Ti–6Al–4V matrix around the 356 μm mesh. Fig. 5(c) shows the II sample, in which the etched Fe-containing interdiffusion zone extends to a diameter of 570 μm, while the Fe wire diameter is decreased to
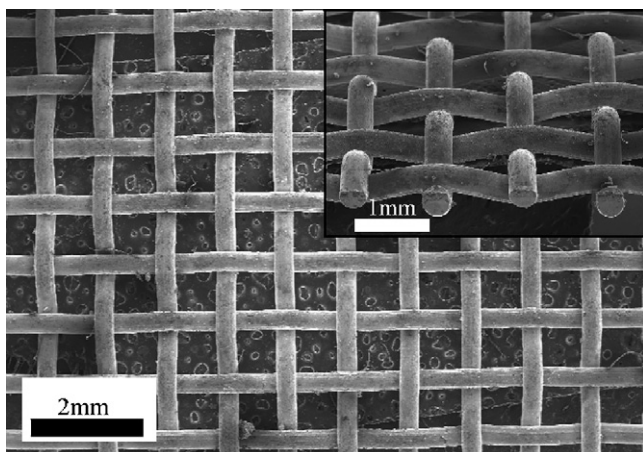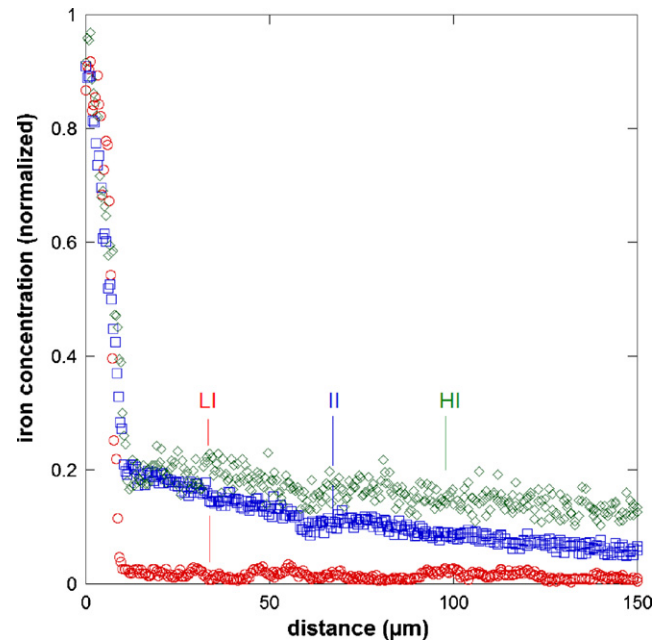
320 μm. Fig. 5(e) for the HI sample shows an etched interdiffusion zone diameter of 740 μm, and a further decrease of wire diameter to 240 μm.

Prior to removing the steel from the titanium alloy matrix, the composites were machined by electro-discharge machining (EDM) into parallelepipeds, exposing the wires to the surface. These samples were then attached to a CP-Ti strip with a nylon wire to maintain electrical contact. The sample, acting as the anode, was then submerged in the center of a beaker with a 0.34 M aqueous sodium chloride solution. Acetic acid, used in Ref. [18], was not used as it was found to pit the Ti–6Al–4V. The cathode was a 500 μm thick sheet of CP-Ti wrapped around the inside circumference of the 84 mm inside diameter beaker to produce a symmetrical, radial electric field. The beaker was then immersed in an ultrasonic bath. The ultrasonic vibration served to remove the loosely adherent iron oxide formed by the electrochemical reaction, while bringing fresh solution to the reacting steel wires deep within the sample. A 2.5 V voltage bias was determined to be optimal: higher values led to concurrent oxidation of both steel and titanium matrix and lower values reduced the rate of dissolution. Dissolution kinetics was measured on a separate sample, with dimensions
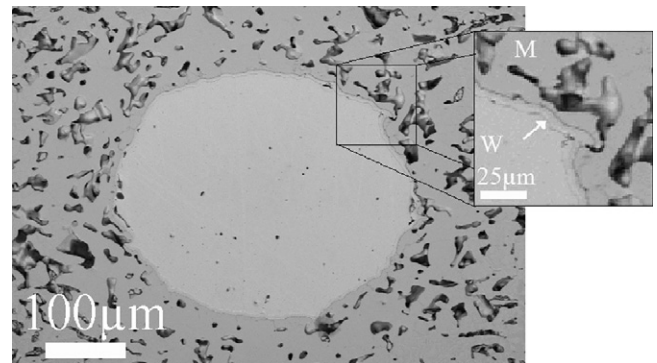

Fig. 2. SEM image of steel mesh, showing orthogonal arrangement of steel wires. Inset: tilted view of steel mesh showing interweaving of wires.

Fig. 4. SEM micrograph of cross-section of sample LI, showing steel wire (W) surrounded by partially densified Ti–6Al–4V matrix (M) with microporosity (black). Interface shows TiC layer (arrow in inset).
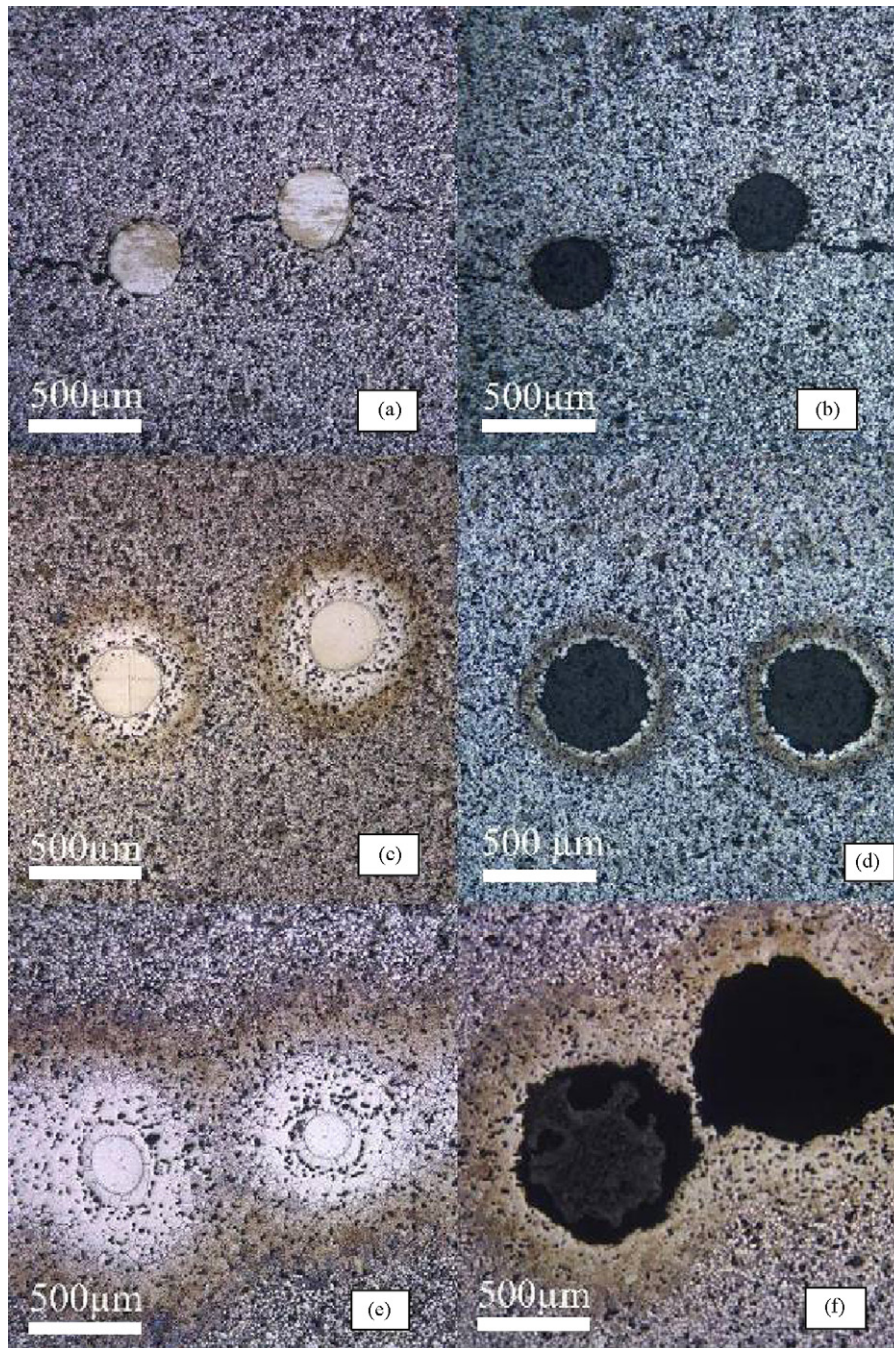
Fig. 5. Optical micrographs of cross-sections polished and etched perpendicular to the meshes for (a), (c) and (e) samples before electrochemical treatment, with two steel wires in light grey color, and (b), (d) and (f) after electrochemical steel removal, with two macropores in black. (a and b) Sample LI with high-carbon steel; (c and d) sample II with low-carbon steel; (e and f) sample HI with low-carbon steel.

of 9 mm × 4.5 mm × 4.5 mm and containing 10 meshes. This sample was produced by hot-pressing for 2 h at 10 MPa with temperature cycled between 860 °C and 1020 °C. Complete removal of the carburized steel wires, as measured by a mass loss of 250 mg, was achieved after 18–21 h. This sample is directly comparable to the LI sintered samples due to its lack of iron diffusion, and it exhibits an average material removal rate of ~1.6 mm³/h. This is higher than the removal rates reported in Ti–6Al–4V for laser machining (0.23 mm³/h for 300 μm holes to 0.127 mm depth [20]) and EDM (0.31 mm³/h for 300 μm diameter holes to 1 mm depth [21]). The present process has several advantages over other microscale perforation methods. Firstly, it is an inherently parallel process, allowing production of multiple holes in one or more samples con-

currently, which can increase the effective material removal rate by orders of magnitude as compared to the laser, microdrilling or EDM processes where each hole must be created sequentially. Also, microdrilling is limited by the strength of the tool, which is greatly decreased at these small size scales, and EDM produces a thin recast layer that can affect the mechanical properties of the samples. Lastly, these other techniques can only produce straight holes with constant cross-section. By contrast, holes replicating ductile steel wires can exhibit various shape, cross-section and tortuosity.

Fig. 5(b) for sample LI exhibits pore diameters which exactly replicate the shape of the 356 μm diameter steel wires, as expected from Fig. 3 and from the results on CP-Ti by Kwok et al. [18].
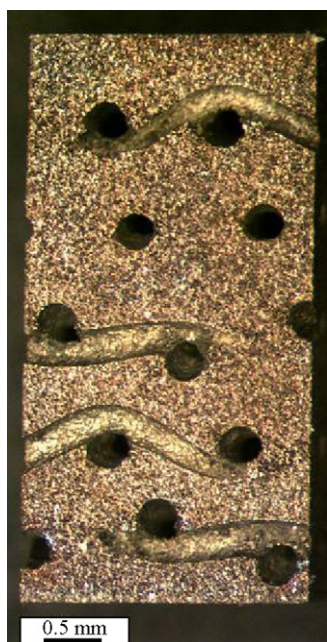
Fig. 6. Photograph of untested LI sample, showing 5 layers of 2D-interconnected macropores.

Fig. 7. Compressive stress–strain curves for the three porous samples, with total porosity indicated.

Fig. 5(d) for sample II shows an increase in pore diameter to 590 μm. Finally, Fig. 5(f) shows pores with a diameter of 920 μm. These figures demonstrate that the dissolution region extends beyond that visible by etching in Fig. 5(a), (c) and (e). However, the diffusion distance of iron in the matrix, as determined from the EDX profiles (Fig. 3), is longer than the dissolution distance resulting in hole diameters of 590 or 920 μm (Fig. 5). The iron-containing zone around the hole is however unlikely to corrode significantly during use, since the dissolution rates at the end of the dissolution process were extremely small, despite a high applied voltage. Further studies are however needed to confirm this hypothesis. Finally, we note that iron additions up to 0.2 wt.% to Ti–6Al–4V may improve the tensile strength and 0.2% yield strength of titanium alloys, [22]. Fig. 5(a)–(f) demonstrates that various levels of porosity, in excess of the fraction of steel wire, can be achieved by varying the sintering time and thus the extent of interdiffusion. The highest pore fraction is however limited, for the present configuration of meshes, by overlapping diffusion lengths between wires, which creates regions with very high local porosity.

Fig. 6 shows a macrograph of an untested compression LI foam, showing five layers of porosity with 12 pores perpendicular to the side face of the sample, and four pores near parallel to the surface, illustrating the waviness of the mesh wires. This sample shows 2D connectivity in each of the five planes where the meshes were embedded. If desired, connectivity in the third dimension (vertical direction in Fig. 6) could be achieved by adding vertical wires that connect with the meshes, or by drilling holes. Total porosity for the HI sample, as determined by the Archimedes method, is p = 41%. Total porosities for the II and LI samples as determined by
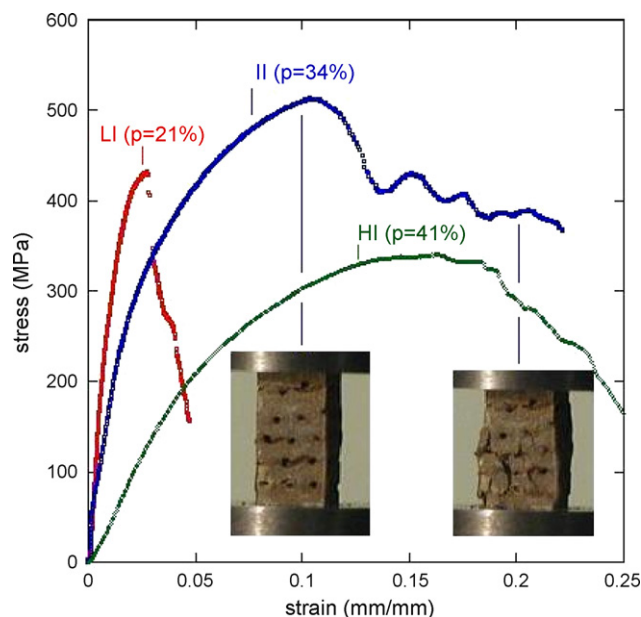
dimensional analysis are p = 34% and 21%, respectively. This total porosity consists of macroporosity, from the electrochemical material removal, and microporosity in the matrix, as shown in Fig. 4. Microporosity was determined by image analysis to represent a volume fraction of 12.6 ± 2.8% within the matrix in all three samples. These micropores exist because of incomplete densification resulting from the low sintering temperature (as compared to the range 1200–1350 °C reported for sintering of Ti–6Al–4V [23,24]), chosen to be safely below the Fe–Ti eutectic at 1085 °C.

Uniaxial compressive testing was performed at a strain rate of 0.1 mm/s, using crosshead displacement to determine strain after taking into account machine stiffness through prior calibration with aluminum samples. Three samples, with dimensions 3.25 mm × 3.25 mm × 6.5 mm (LI and II), and 2.5 mm × 2.5 mm × 5 mm (HI) were first each loaded up to 150 MPa and unloaded to near zero three times along the elastic portion of the stress–strain curve (to sit the sample) before being loaded to failure. The resulting stress–strain curves are shown in Fig. 7 and corresponding mechanical properties are reported in Table 1. As expected, stiffness decreases with increasing porosity. However, sample LI with the lowest porosity (p = 21%) failed prematurely by crumbling. By contrast, sample II (p = 34%), despite its higher porosity, shows a higher strength and higher ductility, failing by shear before crumbling (Fig. 7 inset). Finally, sample HI with the highest porosity (p = 41%) shows a lower strength, as expected from the very high local macroporosity in the layers where the steel meshes were present (Fig. 7). A likely reason for the reduced ductility exhibited by all three foams, and in particular the LI foam, is their 1.2–1.8 wt.% oxygen content (as measured by Wah Chang Analytical Laboratory Services, Albany, OR). It is known [25] that

Table 1
Porosity and compressive mechanical properties of three samples produced. Dense, low oxygen, cast Ti–6Al–4V is listed for comparison.

Sample	Total porosity (%)	Microporosity (%)[a]	Macroporosity (%)[b]	Stiffness (GPa)	Yield strength (MPa)	Peak strength (MPa)
LI	20.7	11.4	9.3	40	265	431
II	33.8	9.5	24.3	15	267	513
HI	41.4	8.4	33.0	5	176	341
Ti–6Al–4V [27,28]	0	0	0	105–116	970	1680

[a] Measured matrix microporosity is 12.6 ± 2.8% for all three samples.
[b] Calculated by subtraction of microporosity from total porosity.

0.8 wt.% oxygen reduces the tensile ductility of CP-Ti to near zero, and some tensile components are expected near the holes during uniaxial compression of the foams. Future work will minimize residual atmospheric gases in the furnace to address this issue.

A model to explain these mechanical properties is beyond the scope of the present paper, since it would require knowledge of the strength and strain-hardening behavior of high-oxygen Ti–6Al–4V, as well as a detailed description of the complex stress state existing in the high porosity, high anisotropy regions of the sample where the elongated pores are located, and in the low-porosity, isotropic matrix regions with the microporosity. It is however instructive to compare the mechanical properties of these porous samples to those of cortical bone, with a stiffness of 12–23 GPa, and a compressive yield strength of 140 MPa [26]. The two high porosity Ti–6Al–4V samples (II and HI) achieve a stiffness matched to (or even below) that of bone, an important goal to prevent stress shielding, while maintaining static yield strength well in excess of bone (in part due to hardening by oxygen), and good ductility in compression (despite the high-oxygen contents). Porous Ti–6Al–4V created by steel wire removal, after further optimization of oxygen content and pore geometry, size and fraction, is thus an interesting candidate for bone implant materials

In summary, composites are created by sintering preforms consisting of Ti–6Al–4V powders in which parallel layers of steel meshes are embedded. Equiaxed, uniformly distributed micropores are present in the Ti–6Al–4V matrix as a result of incomplete powder densification, due to the relatively low sintering temperature used to prevent the formation of a Fe–Ti eutectic phase. Electrochemical removal of the steel results in layers of square arrays of cylindrical macropores open to the surface, replicating the steel meshes. The macropore diameter is the same as the steel wires (if carburized steel is used) or can be increased in a controlled manner by allowing interdiffusion between uncarburized steel and Ti–6Al–4V. The macropore fraction, cross-sectional shape, tortuosity, orientation and connectivity can be easily controlled through the steel meshes. These Ti–6Al–4V materials – with two populations of pores with different shape, size and fraction – exhibit low stiffness, moderate strength and acceptable ductility, making them attractive for bone replacement applications.

Acknowledgements

References

[1] M. Geetha, A. Singh, R. Asokamani, A. Gogia, Progress in Materials Science (2008).
[2] G.H. van Lenthe, M.M.M. Willems, N. Verdonschot, M.C.D. Malefijt, R. Huiskes, Acta Orthopaedica Scandinavica 73 (2002) 630–637.
[3] S. Kujala, J. Ryhanen, A. Danilov, J. Tuukkanen, Biomaterials 24 (2003) 4691–4697.
[4] D.C. Dunand, Advanced Engineering Materials 6 (2004) 369–376.
[5] V.I. Itin, V.E. Ponter, V.N. Khodorenko, M.L. Chobanyan, M.Z. Mirgazizov, E.N. Korosteleva, M.A. Belyalova, Powder Metallurgy and Metal Ceramics 36 (1997) 479–482.
[6] C.M. Zou, E. Zhang, M.W. Li, S.Y. Zeng, Journal of Materials Science—Materials in Medicine 19 (2008) 401–405.
[7] D.J. Sypeck, P.A. Parrish, H.N.G. Wadley, in: D.S. Schwartz, D.S. Shih, H.N.G. Wadley, A.G. Evans (Eds.), Porous and Cellular Materials for Structural Applications, MRS, Pittsburgh, 1998, p. 205.
[8] N.G.D. Murray, D.C. Dunand, Composites Science and Technology 63 (2003) 2311–2316.
[9] N.G.D. Murray, D.C. Dunand, Acta Materialia 52 (2004) 2269–2278.
[10] D.T. Queheillalt, B.W. Choi, D.S. Schwartz, H.N.G. Wadley, Metallugical and Materials Transactions A: Physical Metallurgy and Materials Science 31 (2000) 261–273.
[11] C.S.Y. Jee, N. Ozguven, Z.X. Guo, J.R.G. Evans, Metallurgical and Materials Transactions B: Process Metallurgy and Materials Processing Science 31 (2000) 1345–1352.
[12] N.K. Tolochko, V.V. Savich, T. Laoui, L. Froyen, G. Onofrio, E. Signorelli, V.I. Titov, Proceedings of the Institution of Mechanical Engineers Part L: Journal of Materials-Design and Applications 216 (2002) 267–270.
[13] P. Heinl, L. Muller, C. Korner, R.F. Singer, F.A. Muller, Acta Biomaterialia 4 (2008) 1536–1544.
[14] W.H. Lee, D.A. Puleo, Journal of Materials Science Letters 18 (1999) 817–818.
[15] Y. Li, Z.M. Guo, J.J. Hao, S.B. Ren, Rare Metals 27 (2008) 282–286.
[16] K.A. Erk, D.C. Dunand, K.R. Shull, Acta Materialia 56 (2008) 5147–5157.
[17] Y. Chino, D.C. Dunand, Acta Materialia 56 (2008) 105–113.
[18] P.J. Kwok, S.M. Oppenheimer, D.C. Dunand, Advanced Engineering Materials 10 (2008) 820–825.
[19] T. Momono, T. Enjo, K. Ikeuchi, Isij International 30 (1990) 978–984.
[20] J.S. Lash, R.M. Gilgenbach, Review of Scientific Instruments 64 (1993) 3308–3313.
[21] B.B. Pradhan, B. Bhattacharyya, Proceedings of the Institution of Mechanical Engineers Part B: Journal of Engineering Manufacture 222 (2008) 163–173.
[22] D.J. Simbi, J.C. Scully, Materials Letters 26 (1996) 35–39.
[23] M.M. Dewidar, J.K. Lim, Journal of Alloys and Compounds 454 (2008) 442–446.
[24] O.M. Ivasishin, D.G. Savvakin, F. Froes, V.C. Mokson, K.A. Bondareva, Powder Metallurgy and Metal Ceramics 41 (2002) 382–390.
[25] R. Jaffee, H. Ogden, D. Maykuth, AIME Transactions 188 (1950) 1261.
[26] U. Hansen, P. Zioupos, R. Simpson, J.D. Currey, D. Hynd, Journal of Biomechanical Engineering—Transactions of the ASME 130 (2008).
[27] Q.Z. Li, E.Y. Chen, D.R. Bice, D.C. Dunand, Metallurgical and Materials Transactions A: Physical Metallurgy and Materials Science 39A (2008) 441–449.
[28] G. Welsch, R. Boyer, E.W. Collings, Materials Properties Handbook: Titanium Alloys, ASM International, Materials Park, OH, 1994, p. xxii, 1176.